Theoretical introduction to cross-polarized wave generation

3.1 Introduction

This paragraph introduces theoretically the process of cross-polarized wave generation. An historical introduction is presented in section 4.3.
XPW generation is a four-wave mixing process, governed by the anisotropy of the real part of the crystal third-order nonlinearity tensor $\chi^{(3)}$, where an intense linearly polarized incident wave generates a new linearly polarized wave in the orthogonal direction. This process has important applications as a nonlinear filter to increase the temporal contrast of ultra-short laser pulses and to broaden their spectrum (section 4.2).

In the first section I derive the system of differential equations governing XPW generation and analyze the contribution from different terms. Due to the fact that this nonlinear process is generated in a crystal lattice, these terms depend on the angles of propagation of the waves with respect to the crystal axis. This analysis continues in the second section with the derivation of the system in Hamiltonian form and the analysis of the trajectories in phase space. All these results are derived for monochromatic plane waves. This analysis is then extended for ultra-short pulses. One of the most interesting properties of XPW generation is that the process is automatically phase-matched and is therefore adapted for applications involving ultra-short pulses. For this kind of pulses temporal compression is not trivial and it is interesting to understand the influence of quality of the recompression on the efficiency of the process and on the generated spectrum. This will be presented in the third section for pulses as short as 10 fs. To describe correctly the process for sub-10 fs pulses the propagation in the crystal needs to be taken into account. In this case a system of nonlinear partial differential equations needs to be solved. This is done using a numerical method called the split-step Fourier method and it is the subject of the fourth section.

3.1.1 Cross-polarized wave generation

I start the theoretical description of XPW generation with the wave propagation equation in a dielectric, linearly isotropic, non-magnetic nonlinear medium [12].

$$\Delta\vec{\mathcal{E}} - \frac{n^2}{c^2}\frac{\partial^2\vec{\mathcal{E}}}{\partial t^2} = \mu_0\frac{\partial^2\vec{P}^{NL}}{\partial t^2}, \tag{3.1}$$

where $\vec{\mathcal{E}}$ is the electric field, n the linear index of refraction, c is the vacuum speed of light, μ_0 vacuum permittivity, and $\vec{P}^{NL}\left(\vec{\mathcal{E}}\right) = \varepsilon_0\chi^{(2)}\vec{\mathcal{E}}\vec{\mathcal{E}} + \varepsilon_0\chi^{(3)}\vec{\mathcal{E}}\vec{\mathcal{E}}\vec{\mathcal{E}} + \cdots$ is the nonlinear dielectric polarization. Only the contribution of the third-order susceptibility tensor $\chi^{(3)}$ is considered to obtain:

$$\vec{P}^{NL}\left(\vec{\mathcal{E}}\right) = \varepsilon_0\chi^{(3)}\vec{\mathcal{E}}\vec{\mathcal{E}}\vec{\mathcal{E}}. \tag{3.2}$$

In a Cartesian coordinate system for a plane wave traveling in z-direction it results:

$$\frac{\partial^2\mathcal{E}_i}{\partial z^2} - \frac{n^2}{c^2}\frac{\partial^2\mathcal{E}_i}{\partial t^2} = \varepsilon_0\mu_0\frac{\partial^2}{\partial t^2}\sum_{j,k,l}\chi^{(3)}_{ijkl}\mathcal{E}_j\mathcal{E}_k\mathcal{E}_l, \tag{3.3}$$

where indices i, j, k, l take x, y, z-values. The plane wave for linearly isotropic medium ($k_x = k_y = k_z \equiv k$) in complex notation is written as

$$\begin{aligned}\mathcal{E}_i(z,t) &= \frac{1}{2}E_i(z)\exp\left[-i\left(\omega t - kz\right)\right] \\ &\quad + \frac{1}{2}E_i^*(z)\exp\left[+i\left(\omega t - kz\right)\right].\end{aligned} \tag{3.4}$$

From Eqs. (3.3) and (3.4) and using the slowly-varying envelope approximation the following system of ordinary differential equations can be derived

$$\begin{aligned}\frac{dE_i(z)}{dz} &= i\frac{2\pi}{8n\lambda}\sum_{j,k,l=x}^{z}\chi^{(3)}_{ijkl}[E_j(z)E_k(z)E_l^*(z) \\ &+ E_j(z)E_k^*(z)E_l(z) + E_j^*(z)E_k(z)E_l(z)].\end{aligned} \tag{3.5}$$

In Eq. (3.5) terms corresponding to third harmonic generation are omitted since I consider degenerate third order processes (the other processes are not phase matched and therefore with a very low efficiency). The relation $2\pi/n\lambda = \varepsilon_0\mu_0\omega^2/k$ is used. The third-order susceptibility $\chi^{(3)}_{ijkl}$ is a fourth-rank tensor and has in general 81 elements. Due to the symmetries of the medium most of these terms vanish. The crystals used for XPW generation are cubic crystals (BaF_2, CaF_2, LiF) with m3m cubic symmetry. It is also assumed that the photon energy is below the half band-gap and the two-photon absorption is then neglected. In this case $\chi^{(3)}_{ijkl}$ is a purely real tensor. The $\chi^{(3)}_{ijkl}$-components are usually given in a coordinate system connected with crystalline axes so we assume that (x, y, z) coincide with the corresponding crystalline axes. Components of the electric field of a wave that propagates in the k-direction are however given in a different Cartesian coordinate system (A, B, k). In general (A, B, k) does not coincide with (x, y, z) basis. For definition of angles between the axes of the two coordinate systems see Fig. 3.1. Further I shall refer to the wave E_A with polarization along A-axis as pump or

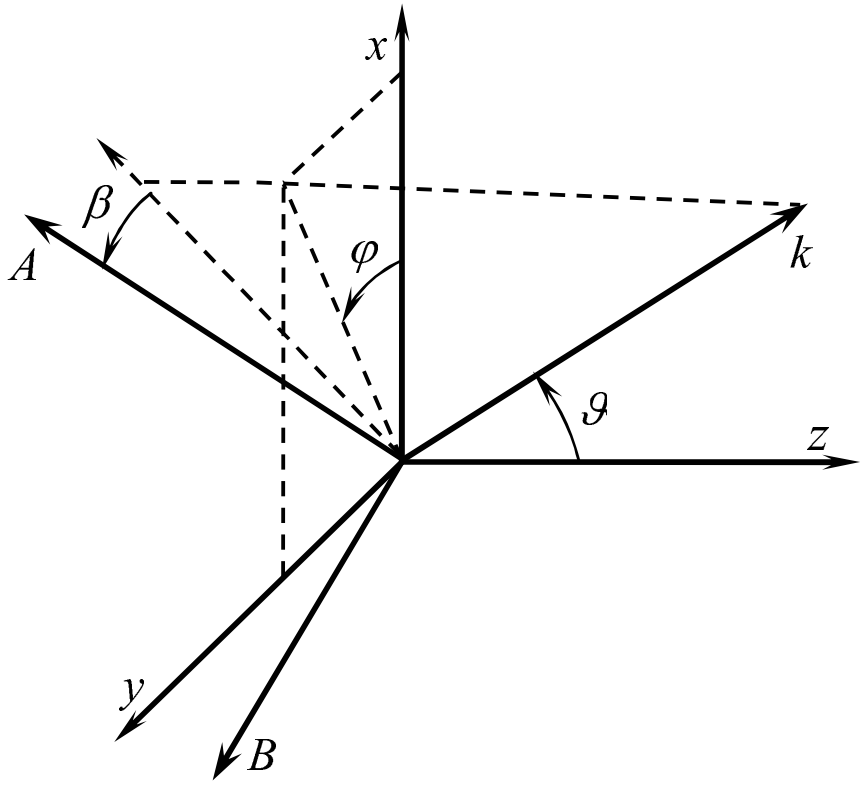

Figure 3.1: Definition of angles. (x, y, z) – basis of the nonlinear crystal, (A, B, k) – light propagation basis. The coordinate system (A, B, k) can be obtained from (x, y, z) by rotating (x, y, z) first around the z-axis by an angle φ, then around the new y axis by θ, and finally by β around the k-axis.

fundamental wave (FW), and to the wave E_B polarized along B-axis (orthogonal to A) as probe wave or XPW. Transformation of coordinates from (x, y, z) to (A, B, k) is given by

$$\begin{pmatrix} E_A \\ E_B \\ E_k \end{pmatrix} = \mathbf{T}(\varphi, \vartheta, \beta) \begin{pmatrix} E_x \\ E_y \\ E_z \end{pmatrix}, \tag{3.6}$$

where the transformation matrix $\mathbf{T}(\varphi, \vartheta, \beta)$ is

$$\mathbf{T}(\varphi, \vartheta, \beta) = \begin{pmatrix} \cos\beta\cos\vartheta\cos\varphi - \sin\beta\sin\varphi & \cos\beta\cos\vartheta\sin\varphi + \sin\beta\cos\varphi & -\cos\beta\sin\vartheta \\ -\sin\beta\cos\vartheta\cos\varphi - \cos\beta\sin\varphi & -\sin\beta\cos\vartheta\sin\varphi + \cos\beta\cos\varphi & \sin\beta\sin\vartheta \\ \sin\vartheta\cos\varphi & \sin\vartheta\sin\varphi & \cos\vartheta \end{pmatrix}. \tag{3.7}$$

First, using the inverse matrix $\mathbf{T}^{-1}$, the components of E_A and E_B waves are derived in (x, y, z)-basis by

$$\begin{pmatrix} E_x \\ E_y \\ E_z \end{pmatrix} = \mathbf{T}^{-1}(\varphi, \vartheta, \beta) \begin{pmatrix} E_A \\ E_B \\ E_k \end{pmatrix} \tag{3.8}$$

and then are substituted in the right-hand side of Eq. (3.5). There is no k-component of the field thus $E_k = 0$ is set. Next, using Eq. (3.7) the derivatives in the left-hand side of Eq. (3.5)

are combined to get back to the system connected with E_A and E_B waves. The following system of differential equations is obtained:

$$\frac{dA(\zeta)}{d\zeta} = i\gamma_1 AAA^* + i\gamma_2 AAB^* + 2i\gamma_2 ABA^* + 2i\gamma_3 ABB^* + i\gamma_3 BBA^* + i\gamma_4 BBB^*, \tag{3.9a}$$

$$\frac{dB(\zeta)}{d\zeta} = i\gamma_5 BBB^* + i\gamma_4 BBA^* + 2i\gamma_4 ABB^* + 2i\gamma_3 ABA^* + i\gamma_3 AAB^* + i\gamma_2 AAA^*. \tag{3.9b}$$

ζ is the longitudinal coordinate in the light propagation direction $\vec{k}$. Polarization of the medium along the k-axis does not generate an electromagnetic wave therefore in Eqs.(3.9) the expression for $dE_k/d\zeta$ is omitted. In Eqs. (3.9) E_A and E_B are denoted simply as A and B, respectively. The γ-coefficients in Eqs. (3.9) depend on the orientation and on the components of the $\chi^{(3)}$-tensor. In the case of crystals with m3m cubic symmetry there are only two independent components [10]: $\chi^{(3)}_{xxxx}$ and $\chi^{(3)}_{xxyy}$. The relation between them is usually defined [10] as $\sigma = \left(\chi^{(3)}_{xxxx} - 3\chi^{(3)}_{xxyy}\right)/\chi^{(3)}_{xxxx}$ and is referred to as the anisotropy of the $\chi^{(3)}$-tensor. For z-orientation, due to the symmetry with respect to rotation around z-axis, there are only three independent nonlinear coupling coefficients since $\gamma_5 = \gamma_1$ and $\gamma_4 = -\gamma_2$. For arbitrary orientation of the nonlinear crystal such relations between coefficients are no longer valid. Instead, the following general relations for the coefficients in the full system (9) may be written

$$\gamma_5(\beta, \varphi, \vartheta) = \gamma_1(\beta + \pi/2, \varphi, \vartheta), \tag{3.10a}$$

$$\gamma_4(\beta, \varphi, \vartheta) = -\gamma_2(\beta + \pi/2, \varphi, \vartheta). \tag{3.10b}$$

The above expressions (3.10) do not convey new physical information. They simply mean that rotating β by 90°, the B-wave would become A, and the A-wave would become B. They could thus serve as a check for the correctness of the derivation of γ coefficients.

Coefficients γ_1 and γ_5 are responsible for self-phase modulation, γ_3 for cross-phase modulation and γ_2 and γ_4 govern the XPW conversion process from A to B and from B to A waves through the last terms in (3.9b) and (3.9a), respectively. This will be shown more clearly in the next section using an Hamiltonian formalism for the XPW generation equations. Note that generally self-phase modulation and XPW generation are not the same for the A and B waves except for z crystallin orientation.

Even in the relatively simple case of cubic crystals explicit expressions for the γ-coefficients as a function of β, φ, and ϑ are quite cumbersome. Here I prefer to take advantage of the transformation matrix $\mathbf{T}$ given in Eq. (3.7) and its inverse matrix $\mathbf{T}^{-1}$ to give more compact expressions for the γ-coefficients:

$$\gamma_1 = \gamma_0 \sum_{j,k=1}^{3} [\delta_{jk} + (1 - \delta_{jk})(1 - \sigma)] T_{1j} T_{j1}^{-1} \left(T_{k1}^{-1}\right)^2, \tag{3.11a}$$

$$\gamma_2 = \gamma_0 \sum_{j,k=1}^{3} [\delta_{jk} + (1 - \delta_{jk})(1 - \sigma)] T_{2j} T_{j1}^{-1} \left(T_{k1}^{-1}\right)^2, \tag{3.11b}$$

$$\gamma_3 = \gamma_0 \sum_{j,k=1}^{3} \left\{ \left[\delta_{jk} + \frac{2}{3}(1-\delta_{jk})(1-\sigma) \right] T_{j2} T_{k1}^{-1} T_{k2}^{-1} + \frac{1}{3}(1-\delta_{jk})(1-\sigma) T_{j1}^{-1} \left(T_{k2}^{-1} \right)^2 \right\} T_{1j}, \tag{3.11c}$$

$$\gamma_4 = \gamma_0 \sum_{j,k=1}^{3} [\delta_{jk} + (1-\delta_{jk})(1-\sigma)] T_{1j} T_{j2}^{-1} \left(T_{k2}^{-1} \right)^2, \tag{3.11d}$$

$$\gamma_5 = \gamma_0 \sum_{j,k=1}^{3} [\delta_{jk} + (1-\delta_{jk})(1-\sigma)] T_{2j} T_{j2}^{-1} \left(T_{k2}^{-1} \right)^2, \tag{3.11e}$$

where $\gamma_0 = 6\pi\chi^{(3)}_{xxxx}/8n\lambda$. δ_{jk} is the Kronecker delta-symbol.

Investigation of Eq. (3.11b) shows that $\gamma_2(\beta, \varphi, \vartheta)$ reaches its global maxima (with equal absolute values of γ_2) when $\varphi = 2n\pi/4$ and $\vartheta = 2(m+1)\pi/4$, or when $\varphi = 2(n+1)\pi/4$ and $\vartheta = 2m\pi/4$ where $m, n = 0, 1, \ldots$. This means that, to reach the maximum of $|\gamma_2|$ for specific values of β-angle, the light propagation direction k should lie in the (x, y), (x, z), or (y, z) plane just between (at 45 degrees) the corresponding crystalline axes. In this respect there are twelve equivalent optimal orientations of the NLC: [110], [$\bar{1}$10], [1$\bar{1}$0], [$\bar{1}\bar{1}$0], [101], [$\bar{1}$01], [10$\bar{1}$], [$\bar{1}$0$\bar{1}$], [011], [0$\bar{1}$1], [01$\bar{1}$], and [0$\bar{1}\bar{1}$], also known as holographic-cut orientations. For the eight equivalent to [111] propagation directions $\gamma_2 = \gamma_4 = 0$ for any angle β and the orthogonal generation term is always zero regardless of the polarization state or orientation, and the medium shows isotropic behavior.

3.1.2 Numerical results

In the non-depleted regime, the efficiency of XPW generation is proportional to the square of γ_2 ([8, 9]). The dependence of this coefficient on angle β is plotted on Fig. 3.2 for three orientations: the most efficient one [101] (holographic-cut), [001] (z-cut), and for the polarization preserving orientation [111] (Fig. 3.3). In calculations $\gamma_0 = 1$ and $\sigma = -1.2$ (typical values for the BaF_2 anisotropy [6]) were used. All the firsts experiments of XPW generation were done using z-cut crystals. This was an academic choice because in this case the k-axis is along the z or equivalent axis. This theoretical analysis demonstrates that the maximum absolute value of γ_2 for [101]-cut is 12% greater than the maximum for z-cut and this corresponds to an almost 26% increase in the XPW efficiency. This advantage does not depend on the particular choice of the values of γ_0 and σ since γ_2 depends linearly on them for arbitrary crystal orientation i.e $\gamma_2 \propto \gamma_0\sigma$.

Calculated values for the coefficients γ_1 and γ_5 for z-cut and holographic-cut crystals are presented in Fig. 3.4. Knowing these coefficients is important since the phase mismatch induced by self-phase modulation impedes efficient XPW generation.

In order to determine the XPW-generation efficiency, the system of differential equations (3.9) is numerically solved. This can be done using standard programs like Matlab, Mathematica, Maple. Analytical information from the equations will be extracted in the next section looking for the trajectories in phase space. In the case of plane-wave propagation the efficiency is defined as the ratio of the intensities of the XPW and the input fundamental wave. The

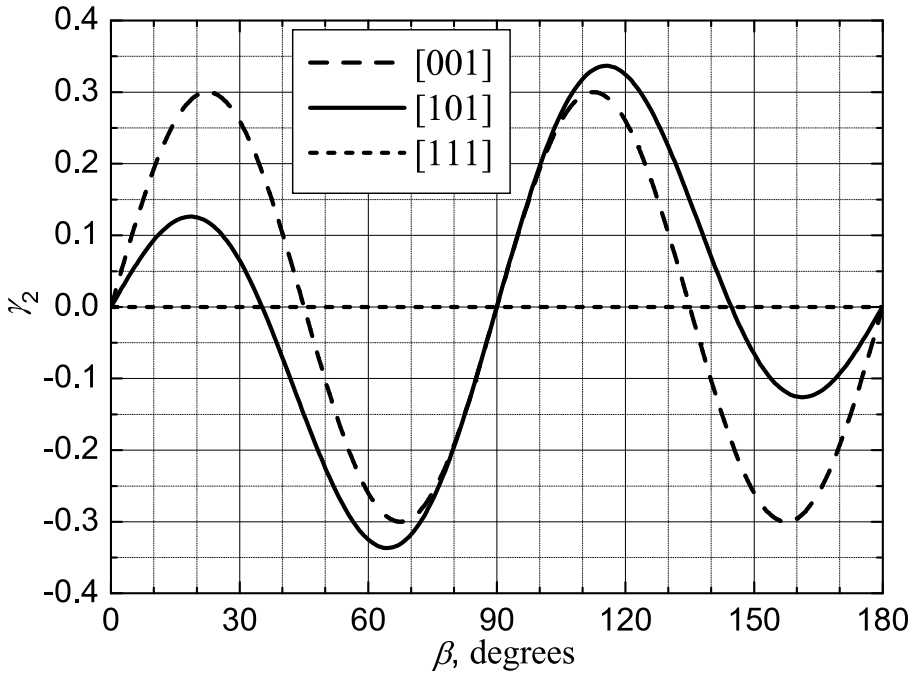

Figure 3.2: Calculated values of γ_2 as function of angle β for different crystal orientations. $\sigma = -1.2$ and $\gamma_0 = 1$.

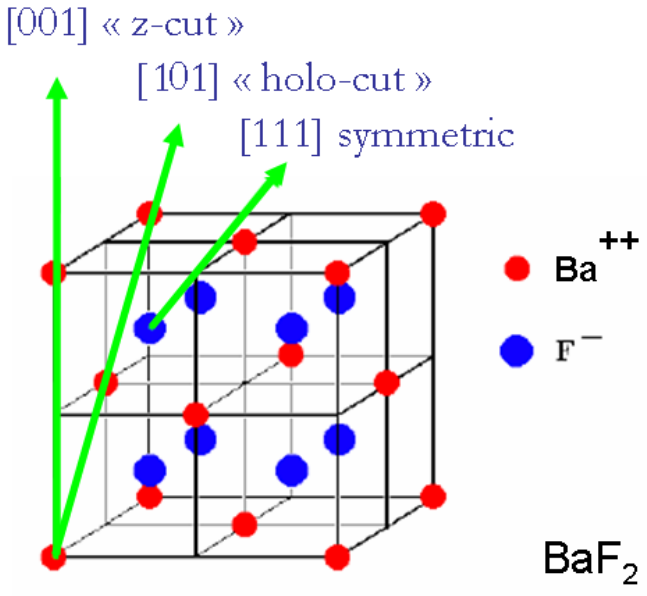

Figure 3.3: Representation of the three different orientations in BaF_2 crystal

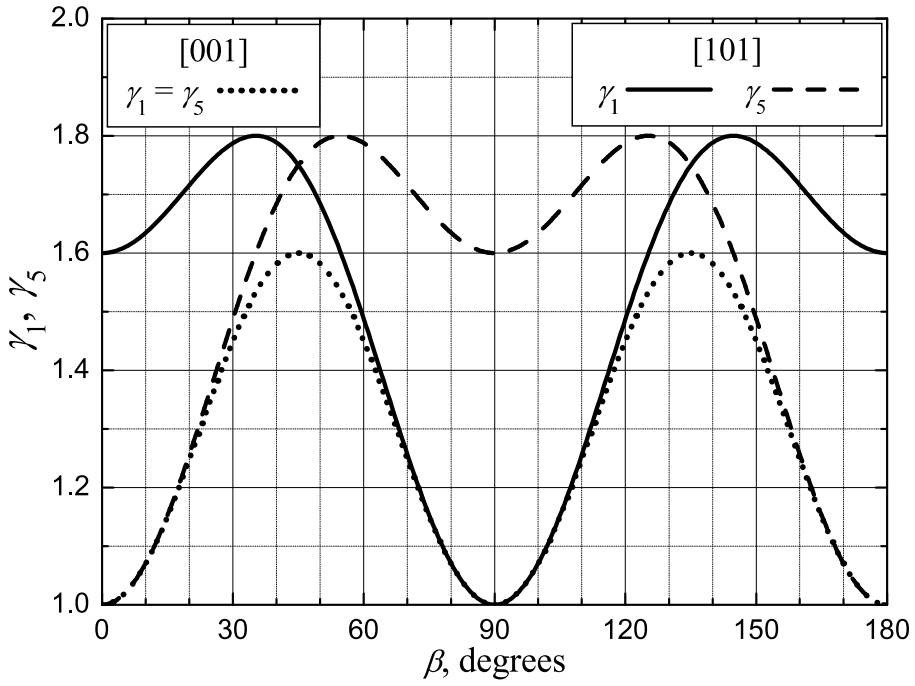

Figure 3.4: Calculated values of γ_1 and γ_5 as function of angle β for z-cut ([001]) and holographic-cut ([101]) crystal orientations. $\sigma = -1.2$ and $\gamma_0 = 1$.

calculated XPW efficiencies for the [101]-cut and for the [001]-cut (z-cut) are shown in Fig. 3.5 along with phase shifts between the fundamental wave and the generated XPW. The dimension-

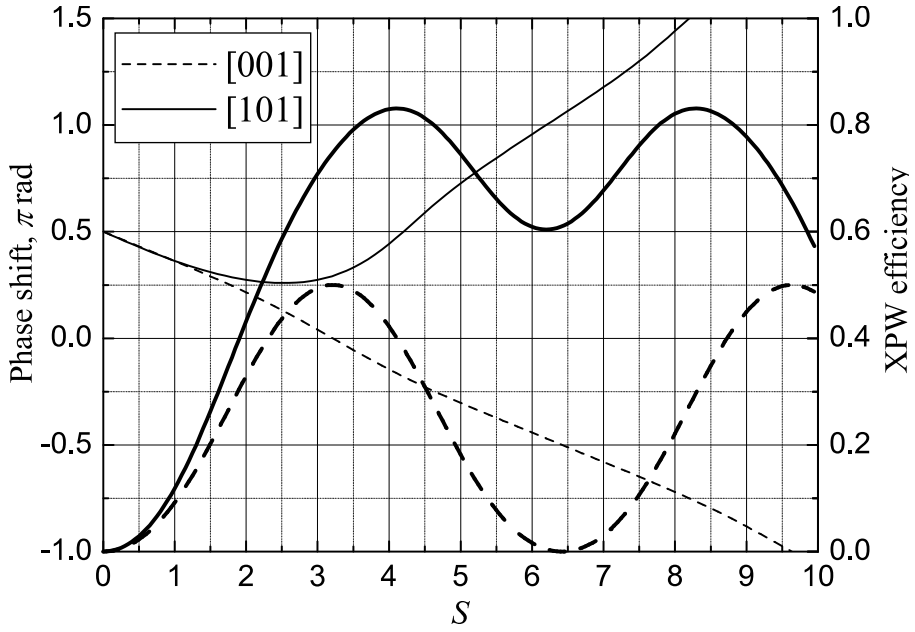

Figure 3.5: Numerically calculated plane-wave XPW efficiency (right scale, thick lines), and phase shift between the fundamental and XPW (left scale, thin lines) for [001] (z-cut) and [101] (holographic-cut) directions of light propagation. $\sigma = -1.2$; $\beta = 22.5°$ for [001] and $\beta = 115.5°$ for [101]-orientation, respectively.

less argument $S = \gamma_0 |A_0|^2 L$, where $A_0 = A(\zeta = 0)$ and L is the crystal length, is proportional to the product of nonlinearity × input intensity × crystal length. The initial condition for the

B-wave is $B(0) = 0$. β-angles used in calculations correspond to the angles at which $|\gamma_2|$ is maximum for each cut (see Fig. 3.2). These angles are optimal for XPW generation at low input intensity.

For z-cut crystals the optimum β depends on the input intensity[9]. This is illustrated in Fig. 3.6(a). At first, it should be noticed that for z-cut crystals there are eight equal maxima

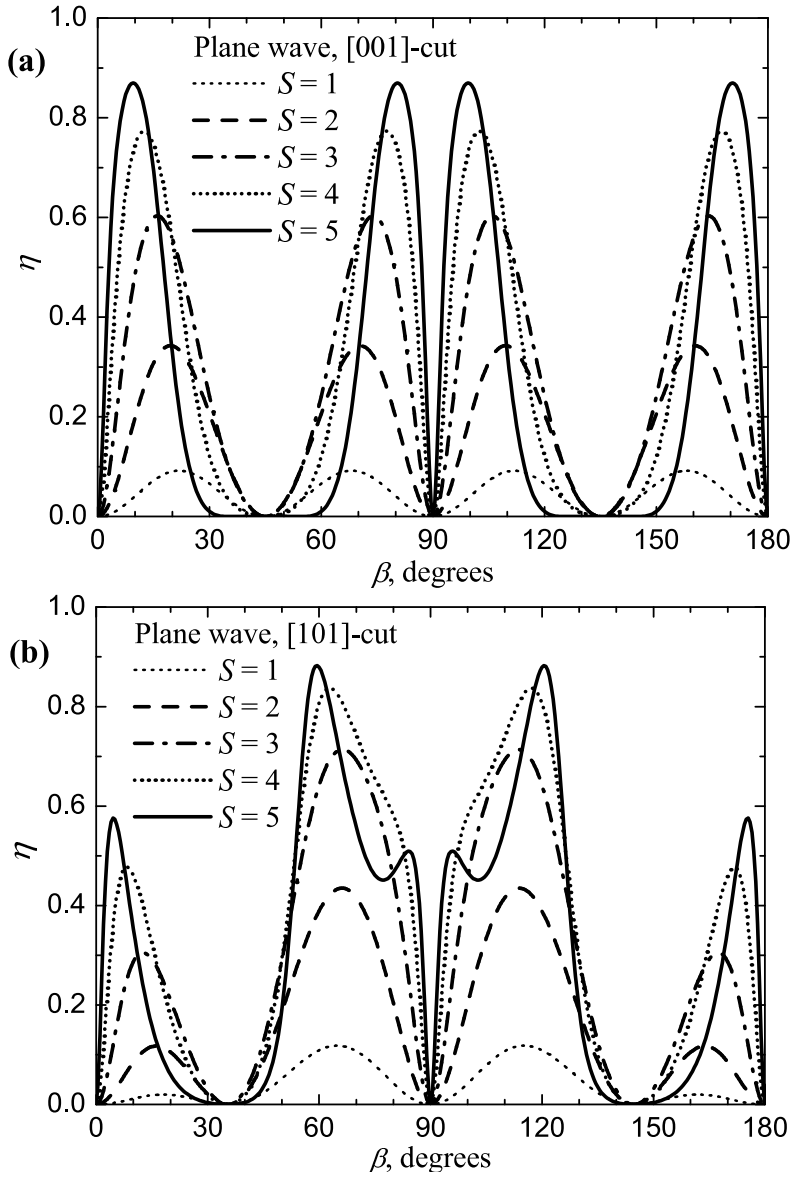

Figure 3.6: Plane-wave XPW efficiency η: (a) for [001]-orientation, and (b) for [101]-orientation as function of angle β for different input intensities. See text for definition of S. $\sigma = -1.2$.

of the generated XPW within 360° rotation of input linear polarization. For any other crystal orientation there are still eight maxima but they are no longer equal – two higher are succeeded by two lower. From Fig. 3.6 it is visible that increasing the input intensities up to $S \approx 5$, the optimal β is shifted by as much as 13 degrees for the z-cut while, for the higher maxima of the [101]-cut, this shift does not exceed 5 degrees. At a slightly lower intensity the shift for [101]-cut becomes very small. The origin of this shift is that the phase mismatch between the fundamental and XPW beam induced by SPM is partly compensated by the shift of β. The

practical experimental limit for the S parameter, $S \approx 5$, [7] can be estimated considering a BaF_2 crystal of few millimeters and a maximum intensity I_0 of $10^{12} W/cm^2$. This maximum intensity corresponds to the threshold for white-light continuum generation [11] for numerical apertures < 0.05 (typical experimental condition). In conclusion, with holographic-cut orientation, the optimum β is almost insensitive to the changes in the intensity for the whole reasonable range of input intensities, which is in contrast to the strong dependence observed with the z-cut. This feature of the holographic-cut orientation together with the higher efficiency make this orientation the most suitable for applications.

The insensitivity of optimum β to the input intensity for holographic-cut orientation is explained by the fact that, compared to the z-cut case, the phase matching conditions for optimal phase shift between the two waves ($\pi/2$) are maintained over a bigger range of input intensities (see Fig. 3.5 left scale, thin lines). The deviation from the optimal phase shift for the holographic-cut is less than $\pi/2$ up to $S = 6$, while at the same conditions the deviation from the optimal phase shift for z-cut is almost π. This insensitivity also means less distortions of the temporal and spatial pulse shape.

Efficiencies shown in Fig. 3.6 are obtained by direct solution of the system (3.9) and are relevant to monochromatic plane waves only. In experiments Gaussian femtosecond pulses are used. Considering the temporal and spatial shapes enables to obtain the energy efficiency of the XPW process. The input beam is assumed with Gaussian spatial and temporal profiles of the form $A(r, t, \zeta = 0) = A_0 \exp(-r^2) \exp(-t^2)$. Diffraction, dispersion, and self-focusing propagation effects are not included in the model. The results for XPW energy efficiencies for [001] and [101] cuts are shown in Fig. 3.7. These curves confirm the advantage of the

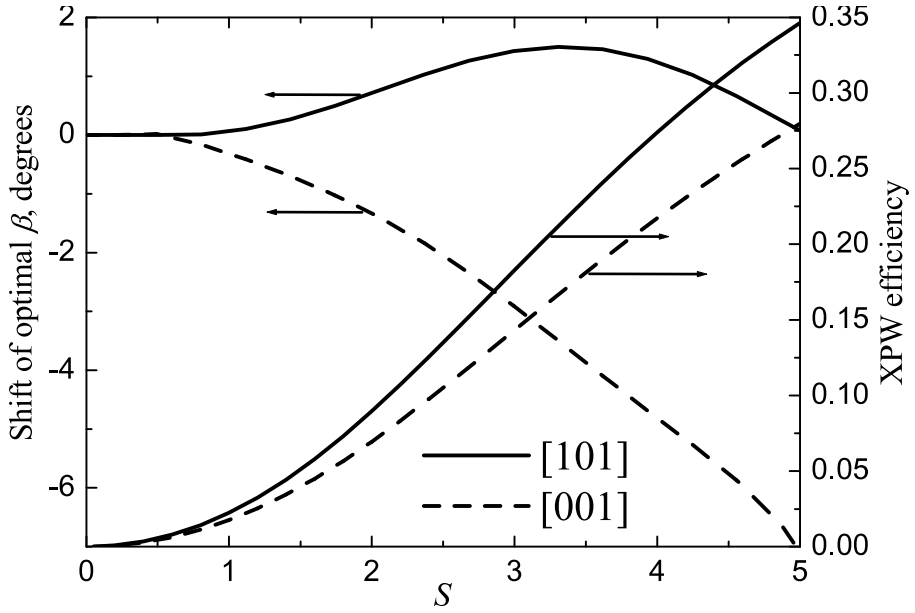

Figure 3.7: XPW efficiencies (right scale) for [001] and [101] orientations assuming Gaussian spatial and temporal profiles of the input beam. Angle β is always optimized for maximum efficiency. The shift of optimum β from its value β_0 for very low input intensity is also shown (left scale). β_0 is 22.5° for [001] and 64.5° for [101] orientation, respectively, and $\sigma = -1.2$.

holographic cut over the z-cut. The ratio of [101] XPW efficiency to [001] XPW efficiency in the range $S = 1 \ldots 5$ is between 1.24 and 1.29, reaching the maximum for $S \approx 1.9$. On the same figure the shift of optimum β from the low-intensity value is also shown. With $S = 5$ an XPW efficiency of more than 30 % can be obtained with the [101] cut. As it will discussed in section 4.4, this efficiency cannot be achieved experimentally in a single crystal but with a two crystals configuration.

3.2 Hamiltonian approach

3.2.1 Introduction

The motivation behind this alternative formulation of the XPW generation system of equations is to extract as much information as possible from the system without solving it numerically. The approach is to start from the general complex system of XPW equations (3.9)(or some simplified version) and to separate the real and imaginary part to obtain the real evolution equations for the amplitude of the two waves and their phase difference. From this system of equations we can derive two quantities that are conserved (first integrals) which are the energy and the momentum. These conserved quantities can be used to solve the problem analytically with some simplifying hypothesis. The conserved momentum is the Hamiltonian of the system and so the real XPW system can be expressed in Hamiltonian form for two conjugate quantities. This is very useful because, as in classical mechanics, the Hamiltonian can be plotted in phase space to derive topological information about the solutions of the differential system of equations without solving it. Furthermore an arbitrary polarization state can be considered. A comparison between z-cut and holographic cut is then made.

3.2.2 Simplified version : only γ_2

I start working with a simplified version of the system (3.9) where I consider just γ_2. In this approximation I just allow the conversion of energy from the fundamental to the XPW beam without any contribution of the self and cross phase modulation (γ_1, γ_5, γ_3). Neglecting γ_4 the system is made fundamentally asymmetric because there is no energy flux if the fundamental is initially zero (no back conversion). Even if this system is simplified it is close to the experimental condition at low intensity (initial condition with just the fundamental beam as input, thin crystals) and the form of the equation is very similar to that used to treat three-wave interactions hence a comparison can be made [2, 4, 3, 5]. To obtain a real system of equations I define the input field A and the XPW field B as: $A = r_1 e^{i\varphi_1}$, $B = r_2 e^{i\varphi_2}$ and $\theta = \varphi_1 - \varphi_2$. Substituting in (3.9) and considering just γ_2 it results:

$$\begin{aligned} \dot{r_1} &= r_1^2 r_2 \gamma_2 sin(\theta) \\ \dot{r_2} &= -r_1^3 \gamma_2 sin(\theta) \\ \dot{\theta} &= 3\gamma_2 r_1 r_2 cos(\theta) - \frac{r_1^3}{r_2}\gamma_2 cos(\theta) \end{aligned} \tag{3.12}$$

with the notation $\frac{dr_i}{d\zeta} = \dot{r}_i$. This system of equation has two constants: the first $r_1^2 + r_2^2 = const$ is the Manley-Rowe relation and it expresses the conservation of the photon flux. Working with normalized quantities the constant is equal to 1. The second is the Hamiltonian of the system $\Gamma = \gamma_2 r_1^3 r_2 cos(\theta)$. Here and in the following calculations the expression for the Hamiltonian is obtained starting with a guess expression and than verifying that the condition $\dot{\Gamma} = 0$ is satisfied. The use of the term 'Hamiltonian' immediately suggests that the conserved quantity is energy, as in classical mechanics. However an analogy is being used when the coupling equations are recognized as being in "Hamiltonian form": the space variable ζ here plays the role of time in the classical mechanics formalism. Since time invariance leads to conservation of energy, it is not surprising that the Hamiltonian in this case is momentum since the conservation of momentum is related to system property invariance in the spatial coordinate [1].

The most typical configuration for XPW generation consists of a single beam (fundamental beam) incident on the nonlinear medium (cubic crystal). In this case the initial condition is $r_1^2 = 1$ and $r_2^2 = 0$ and so $\Gamma = 0$. But $\Gamma = 0$ is a first integral of the system so it will remain zero also when r_1^2 and r_2^2 will be different from zero. The consequence is that $\theta = \pm\pi/2$. In this case $\sin(\theta) = \pm 1$ and the system (3.12) can be further simplified:

$$\dot{r_1} = r_1^2 r_2 \gamma_2 \tag{3.13}$$

$$\dot{r_2} = -r_1^3 \gamma_2 \tag{3.14}$$

and has solutions of the form: $r_1(\zeta) \propto \sqrt{\frac{1}{1+\zeta^2}}$ and $r_2(\zeta) \propto \sqrt{\frac{\zeta^2}{1+\zeta^2}}$. These solutions, derived analytically, have the same asymptotic behavior as the well-known hyperbolic tangent and secant solutions for the SHG process in the case of perfect phase matching. (Fig. 3.8) [2].

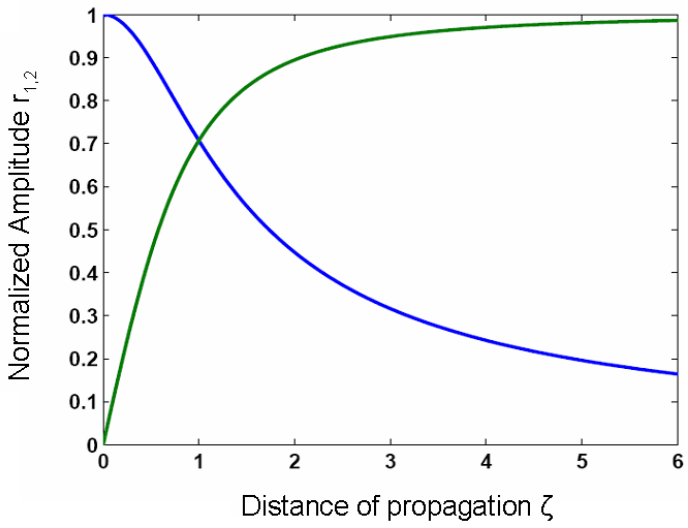

Figure 3.8: Aperiodic energy exchange between the fundamental (blue) and cross-polarized beam (green)

The equation for θ can be expressed using Γ to obtain:

$$\dot{\theta} = 3\gamma_2 \frac{\Gamma}{r_1^2} - \gamma_2 \frac{\Gamma}{r_2^2} \tag{3.15}$$

and so for $\Gamma = 0$, confirmation is given that $\theta(\zeta) = const = \pm\pi/2$. There is an aperiodic transfer of energy between the fundamental and the XPW beam with constant phase difference. The same occurs for r_1^2 and r_2^2 different from zero and $\theta = \pm\pi/2$. For a more general situation the system (3.12) can be written in the form :

$$\zeta = \int_{r_2^2(0)}^{r_2^2(\zeta)} \frac{d(r_2^2)}{(r_2^2(1-r_2)^3 - \Gamma^2)^{1/2}} \tag{3.16}$$

which is an elliptical integral of the first type. The solutions can be expressed in terms of Jacobi elliptic function and are in general periodic (we have seen previously a particular situation where this is not true). It is not very interesting to enter into the mathematical details of these solutions because more can be understood by working with the system in Hamiltonian form. Defining $\eta = r_1^2$ and using the Manley-Rowe relation (const=1) the system (3.12) is written in Hamiltonian form:

$$\frac{d\eta}{dz} = -2\frac{\partial \Gamma}{\partial \theta} \tag{3.17}$$

$$\frac{d\theta}{dz} = 2\frac{\partial \Gamma}{\partial \eta} \tag{3.18}$$

with $\Gamma = \gamma_2 \eta^{3/2}(1-\eta)^{1/2} cos(\theta)$. η and θ are conjugate variables and a phase space can be defined (Fig. 3.9). For this plot it is assumed a propagation with an angle β corresponding to a maximum of γ_2 at low intensity. The observation of the trajectories in phase space highlights some of the more general properties of the solutions. No information function of z can be extracted because the differential system of equations is not solved. Due to the Manley-Rowe relation, information about the XPW signal is directly extracted from the variation of η ($r_2^2 = 1-\eta$). We see that in phase space there are two separatrix (vertical trajectories) for $\theta = \pm\pi/2$; these correspond to the solutions we have derived in the case of $\eta = 1$ as input, where there is an exchange of energy between the two waves with constant phase difference. Separatrix illustrate the aperiodic nature of the conversion. Between this two separatrix we have closed orbits where η and θ are periodic functions. These correspond to the Jacobi elliptical functions. The center of the closed orbits are points where both η and θ remains constant, these are the eigensolution of the system and they can be obtained by imposing $\frac{d\eta}{dz} = \frac{d\theta}{dz} = 0$.

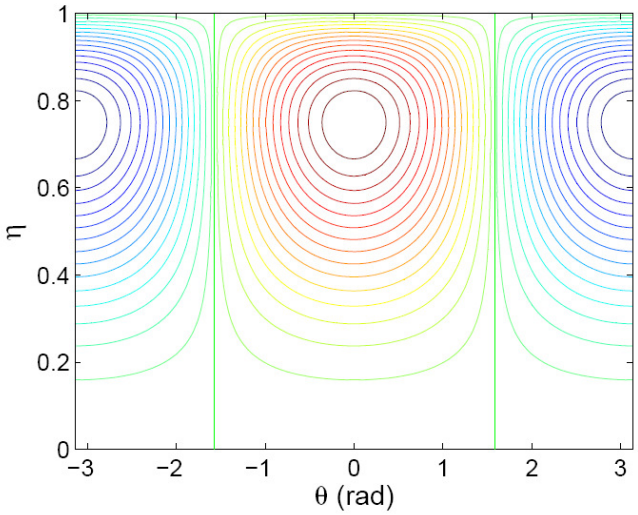

Figure 3.9: Hamiltonian in phase space for the simplified system (just γ_2). Trajectories $\Gamma(\eta, \theta) = const$ in phase space correspond to solutions of the differential system of equations for XPW generation.

3.2.3 Extension of the analysis

This analysis can then be extended including one by one the missing terms for the complete description of the XPW process. The first step is to work with a symmetric system and so consider the presence of both γ_2 and γ_4. Repeating the same procedure described in the previous section the same system of equations (3.18) is obtained with: $\Gamma = \gamma_2\eta^{3/2}(1-\eta)^{1/2}cos(\theta) + \gamma_4\eta^{1/2}(1-\eta)^{3/2}cos(\theta)$.

I start the phase space analysis of the trajectories by considering XPW generation in Z-cut crystals where $\gamma_4 = -\gamma_2$. As it can be seen from the trajectories reported in fig. 3.10 the form of the solution is equal to what I have discussed in the previous paragraph except from the fact that now the problem is perfectly symmetric between the fundamental and the XPW beam and only half of the energy can be at maximum transferred. When there is just one input beam, $\Gamma = 0$, and the solution moves along the separatrix with constant phase difference. Circular polarization ($\eta = 0.5, \theta = \pm\pi/2$) is an eigensolution of the system because it corresponds to a saddle point in phase space. Fig. 3.11 shows the trajectories in phase space for XPW generation in holo cut crystals $\gamma_4 \neq -\gamma_2$. As in the previous plot the propagation is assumed with an angle *beta* which maximizes γ_2 (this angle is different from previous one). The type of trajectories is the same that for Z-cut with the exception that circular polarization is not an eigensolution of the system. Furthermore the energy transfer between the to beam can reach 65%.

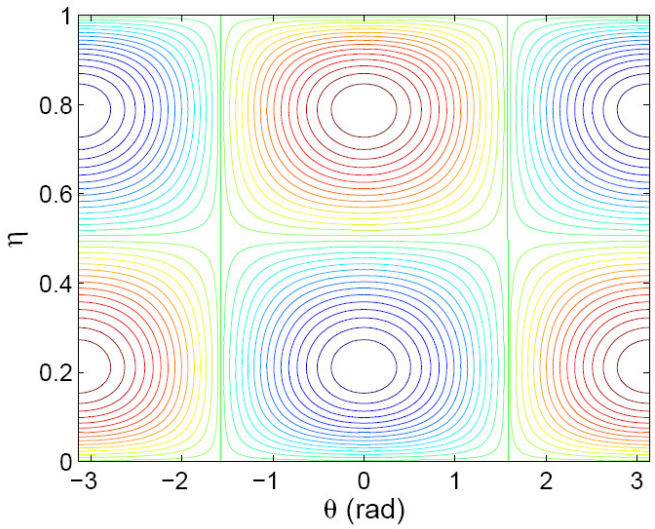

Figure 3.10: Hamiltonian in phase space and corresponding orbits for the system with γ_2 and γ_4 (Z-cut $\beta = \pi/8$).

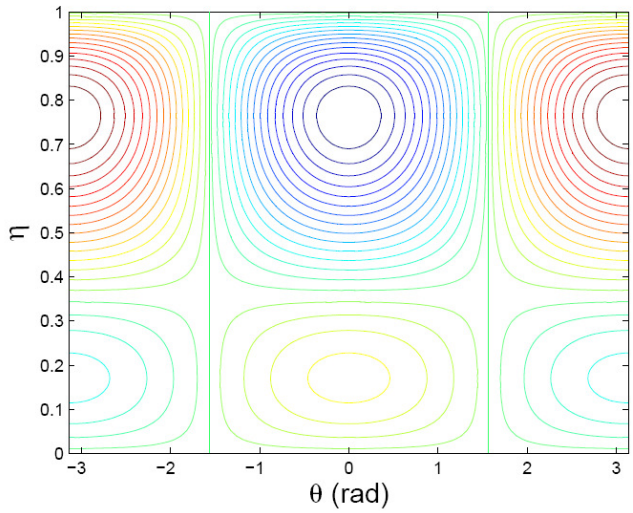

Figure 3.11: Hamiltonian in phase space and corresponding orbits for the system with γ_2 and γ_4 (Holo-cut $\beta = (115.5)$.

Including self-phase modulation of the fundamental beam means considering also the presence of γ_1 in the XPW system of equations. The Hamiltonian in this case is:

$$\Gamma = \gamma_2 \eta^{3/2}(1-\eta)^{1/2} cos(\theta) + \gamma_4 \eta^{1/2}(1-\eta)^{3/2} cos(\theta) + \frac{\gamma_1}{4}\eta^2 \tag{3.19}$$

Because there is no substantial difference between different cuts of the crystal, results about Z-cut only are presented. This problem can be solved analytically by neglecting depletion of the fundamental [9]. Fig. 3.12 shows the trajectories in phase space. There are two kind of trajectories: the closed orbits where the amplitude and the phase difference is periodic and the open orbits where the amplitude is periodic but the phase is not periodic. This new kind of solution is allowed in the system due to the presence of self phase modulation and this is

exactly the solution we have in practical experimental XPW generation at high intensity(just one input beam, $\theta_{in} = -\pi/2$). There is no longer the presence of separatrix and so transfer of energy with constant phase difference is not possible anymore. Comparing the Hamiltonian (3.19) to the one that can be derived for a Hamiltonian treatment of three-wave mixing, it is evident that the γ_1 term in XPW generation acts like the phase matching terms (except that here η is squared) with the generation of open orbits in phase space.

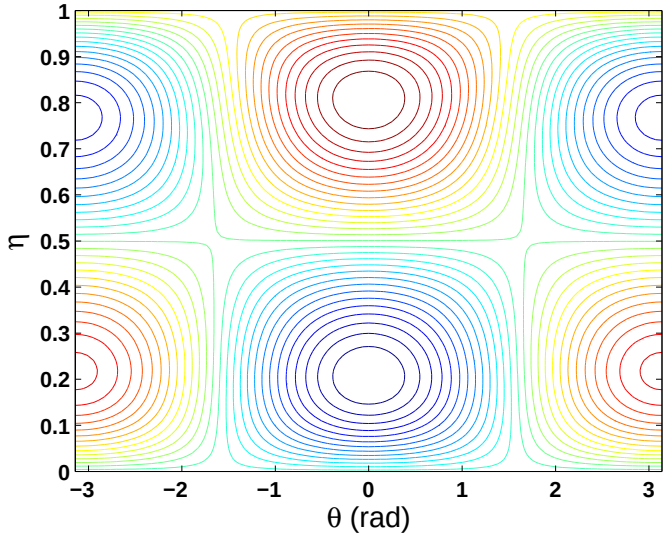

Figure 3.12: Hamiltonian in phase space and corresponding orbits for the system with γ_2 and γ_4 and γ_1 (Z-cut $\beta = \pi/8$).

The solutions of the complete problem expressed in (3.9) can now be addressed. The procedure to obtain the hamiltonian of the system consists, as previously presented, in obtaining the real system of equations starting from the complex system (separating the real and imaginary parts) and then finding the first integral (constant of motion) of the problem. The Hamiltonian is:

$$\begin{aligned} \Gamma = \gamma_2\eta^{3/2}(1-\eta)^{1/2}cos(\theta) + \gamma_4\eta^{1/2}(1-\eta)^{3/2}cos(\theta) + \\ +\gamma_3\eta(1-\eta)cos(2\theta)/2 + \frac{\gamma_1}{4}\eta^2 - \frac{\gamma_3}{2}(1-\eta)^2 - \frac{\gamma_3}{2}\eta^2 + \frac{\gamma_5}{4}(1-\eta)^2 \end{aligned} \tag{3.20}$$

where I have kept separated the contributions from different gamma. The plot of the trajectories in phase space is reported in Fig. 3.13 Fig. 3.14 for Z-cut and holo cut respectively. The same type of trajectories that I have discussed for the previous cases is present. In particular, depending on the relative (amplitude/phase) relation between the two orthogonal input waves, there are closed orbits with periodic oscillation of the amplitude and open orbits with periodic amplitude but not periodic phase. There are also different eigensolutions of the system (constant amplitude and phase) that can be divided into stable and unstable. Finding the stability of an eigensolution directly from the phase space plot is another advantage of the Hamiltonian approach. For example we can see that circular polarization is an eigensolution for Z-cut also in the presence of self and cross phase modulation but that this solution is unstable (saddle

point in phase space). For Holo cut we have the same kind of trajectories as discussed for Z-cut (but with a different angle β) and, due to the asymmetry in the η axis, circular polarization is not an eigensolution of the system.

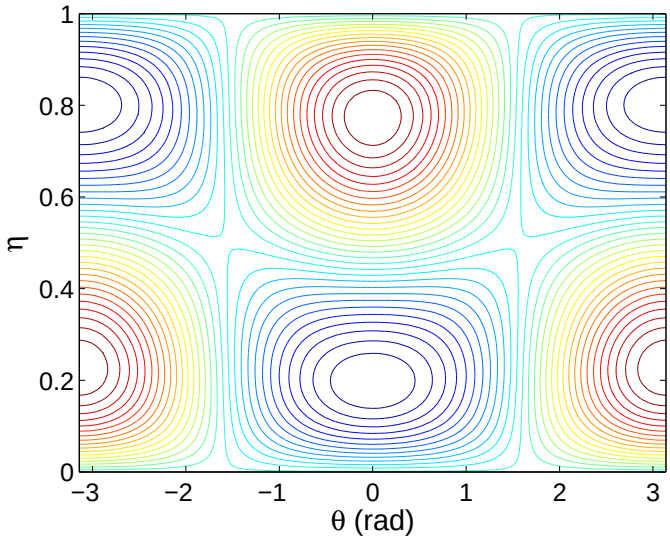

Figure 3.13: Hamiltonian in phase space and corresponding orbits for the complete system of equations and for Z-cut ($\beta = \pi/8$).

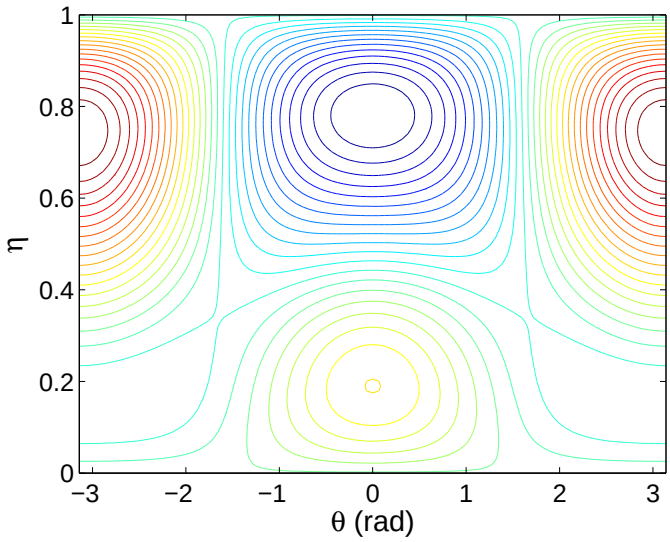

Figure 3.14: Hamiltonian in phase space and corresponding orbits for the complete system of equations and for Holo-cut ($\beta = (3/8 - 0.0168)\pi$).

Bibliography

[1] N. A. Ansari, C. Pask, and D. R. Rowland. Momentum in nonlinear optics. *Journal of Modern Optics*, 47(6):993–1011, 2000.

[2] J. A. Armstrong, N. Bloembergen, J. Ducuing, and P. S. Pershan. Interactions between light waves in a nonlinear dielectric. *Phys. Rev.*, 127(6):1918–1939, 1962.

[3] A. Bandilla, G. Drobný, and I. Jex. Phase-space motion in parametric three-wave interaction. *Optics Communications*, 128(4-6):353 – 362, 1996.

[4] A. Bandilla, G. Drobný, and I. Jex. The classical parametric approximation for three-wave interactions. *Optics Communications*, 156(1-3):112 – 122, 1998.

[5] N. Forget PhD manuscript.

[6] M. Dabbicco, A. M. Fox, G. von Plessen, and J. F. Ryan. Role of $\chi^{(3)}$ anisotropy in the generation of squeezed light in semiconductors. *Phys. Rev. B*, 53:4479–4487, 1996.

[7] A. Jullien, O. Albert, G. Chériaux, J. Etchepare, S. Kourtev, N. Minkovski, and S. M. Saltiel. Two crystal arrangement to fight efficiency saturation in cross-polarized wave generation. *Opt. Express*, 14:2760–2769, 2006.

[8] N. Minkovski, G. I. Petrov, S. M. Saltiel, O. Albert, and J. Etchepare. Polarization rotation induced by cascaded third-order processes. *Opt. Lett.*, 27:2025–2027, 2002.

[9] N. Minkovski, G. I. Petrov, S. M. Saltiel, O. Albert, and J. Etchepare. Nonlinear polarization rotation and orthogonal polarization generation experienced in a single-beam configuration. *J. Opt. Soc. Am. B*, 21:1659–1664, 2004.

[10] G. Petrocelli, E. Pichini, F. Scudieri, and S. Martellucci. Anisotropic effects in the third-harmonic-generation process in cubic crystals. *J. Opt. Soc. Am. B*, 10:918–923, 1993.

[11] Th. Schneider and J. Reif. Influence of an ultrafast transient refractive-index grating on nonlinear optical phenomena. *Phys. Rev. A*, 65(2):023801, Jan 2002.

[12] A. Yariv and P. Yeh. *Optical waves in crystals*. Wiley, New York, 1984.

3.3 XPW for short pulses

Introduction

In the previous sections XPW generation is treated in the time domain and using monochromatic plane waves equations. For the applications of this process as a contrast filter it is interesting to extend this analysis to ultra-short pulses. The quality of temporal pulse compression for ultra-short pulses is typically given in the frequency domain as a residual spectral phase that is expanded in a Taylor series around the central frequency. As is known for other nonlinear effects this spectral phase affects the output (efficiency, spectral width and spectral shape) of the process. It is thus interesting to express and solve the envelope equations of the process in the frequency domain. This is done by making some simplifications and is presented in the next sections. Before entering this subject I want to have a brief discussion about the response time of XPW generation. For optical frequencies non resonant with the optical medium, the response time of the nonlinear susceptibility is given by the time needed for an electron, excited by an oscillating electric field, to come back to the equilibrium position. If $\triangle\omega$ defines the difference in energy between the electromagnetic pulsation and the conduction band (or more generally the energy of the first ionization threshold), the life time τ of the electron out of equilibrium is given by the uncertainty relation:

$$\Delta E\tau \backsim \hbar \tag{3.21}$$

For all crystals used for XPW generation, $\triangle E \approx 10eV$ ($\triangle E_{BaF2} = 9.21$ eV, $\triangle E_{CaF2} = 9.92$ eV, $\triangle E_{LiF} = 11.6$ eV). It results that τ is <1 fs and thus much shorter than few-cycle optical pulses. XPW generation is then always considered an instant process.

3.4 Theoretical considerations: Spectral approach

3.4.1 Notations

For practical reasons linked to the fact that the XPW process leads to a strong pulse reshaping, the XPW spectrum is characterized by its statistic moments rather than central wavelength and FWHM spectral width. The following formulas are used to evaluate respectively the energy, spectral width and center of mass of a given spectral distribution $I(\omega)$:

$$E_{\mathrm{I}} = \int_{\mathbb{R}} I(\omega)d\omega \qquad \sigma_{\mathrm{I}}^2 = \frac{\int_{\mathbb{R}} \left(\omega - <\omega>_{\mathrm{I}}\right)^2 I(\omega)d\omega}{\int_{\mathbb{R}} I(\omega)d\omega} \qquad <\omega>_{\mathrm{I}} = \frac{\int_{\mathbb{R}} \omega I(\omega)d\omega}{\int_{\mathbb{R}} I(\omega)d\omega} \tag{3.22}$$

These parameters are not only universal and easy to define but also of first interest from an experimental point of view: the efficiency of the nonlinear process defines the output energy, the standard deviation defines the minimum available transform limited pulse duration and the spectral center of mass shift indicates whether the XPW spectrum still lies within the amplification bandwidth of a laser amplifier. More generally, the mean value of the spectral

function f(ω) with respect to the intensity I(ω) is defined by:

$$< f(\omega) >_{\mathrm{I}} = \frac{\int_{\mathbb{R}} f(\omega) I(\omega) d\omega}{\int_{\mathbb{R}} I(\omega) d\omega} \tag{3.23}$$

3.4.2 Propagation equation

The effect of spectral phase on a nonlinear process has been extensively studied theoretically for $\chi^{(2)}$ processes [15, 16, 17, 18, 19]. In this section this study is extended to $\chi^{(3)}$ processes and more specifically to XPW generation. The starting point is the plane wave propagation equations describing XPW generation (3.9) considering just the influence of γ_2. As previously ω_0 stands for the central angular frequency of the input pulse (fundamental pulse), n for the refractive index of the cubic crystal at ω_0, $\chi^{(3)}$ for the third order susceptibility tensor, β for the angle between the input polarization direction and the crystallographic axis x, $A(z,t)$ and $B(z,t)$ for the respective complex amplitude envelopes of the fundamental and XPW electric fields, $I_A(z,\omega)$ and $I_B(z,\omega)$ for the respective spectral intensity of the fundamental and XPW electric fields. Here the anisotropy factor of the third order susceptibility tensor is defined σ_x to avoid confusion with the second order momentum of a Gaussian function. The spectral phase function of the fundamental pulse will be referred as $\varphi(\omega)$ and, when required, $\varphi(\omega)$ will be expanded in a Taylor series around ω_0:

$$\varphi(\omega) = \sum_{k=0}^{n} \frac{\varphi^{(k)}}{k!} (\omega - \omega_0)^k . \tag{3.24}$$

In the frame of the moving pulse, the slowly varying envelope approximation leads to the following propagation equation for the complex amplitude of the XPW field:

$$\frac{\partial B(z,t)}{\partial z} = i\gamma_2 A(z,t) A^*(z,t) A(z,t) \tag{3.25}$$

$$\text{with } \gamma_2 = -\frac{3}{8} \frac{\omega_0}{n_0 c} \chi^{(3)}_{xxxx} \frac{\sigma_x}{4} \sin(4\beta) \tag{3.26}$$

Using the standard Fourier transform $B(z,t) = \int_{\mathbb{R}} \tilde{B}(z,\omega) \exp(i\omega t) d\omega$ and $A(z,t) = \int_{\mathbb{R}} \tilde{A}(z,\omega) \exp(i\omega t) d\omega$ and applying the reverse convolution theorem we obtain the following equation for the complex spectral amplitude of the XPW pulse:

$$\frac{\partial \tilde{B}(z,\omega)}{\partial z} = -i\gamma_2 \iint_{\mathbb{R}^2} \tilde{A}(z,\omega_1) \tilde{A}(z,\omega_2) \tilde{A}^*(z,\omega_1+\omega_2-\omega) d\omega_1 d\omega_2 \tag{3.27}$$

Equation (3.27) highlights the frequency-mixing process occurring during XPW generation: the XPW signal at a given angular frequency is proportional to some third order spectral autocorrelation function of the fundamental pulse. In the approximation of small conversion efficiency (undepleted regime) and of negligible dispersion, the fundamental pulse propagates unchanged ($A(z,t) = A(0,t) = A(t)$) and equation (3.27) can be solved analytically:

$$\tilde{B}(L,\omega) = -i\gamma_2 L \iint_{\mathbb{R}^2} \tilde{A}(\omega_1) \hat{A}(\omega_2) \tilde{A}^*(\omega_1+\omega_2-\omega) d\omega_1 d\omega_2 \tag{3.28}$$

3.4.3 Gaussian pulse with quadratic phase

For a fundamental pulse of Gaussian spectral intensity, the spectral amplitude is:

$$\tilde{A}(\omega) = \tilde{A}_0 \exp\left(-\frac{(\omega-\omega_0)^2}{2\sigma^2}\right) \exp\left[i\varphi(\omega)\right] \tag{3.29}$$

with the spectral phase defined as in (3.24). The right hand side of equation (3.28) can be solved analytically for the specific case of a quadratic phase. The result for the spectral intensity in this case is:

$$I_B(L,\omega) = \left(2\pi\sigma^2\tilde{A}_0^3\gamma_2 L\right)^2 \frac{\exp\left[-\frac{(\omega-\omega_0)^2}{3\sigma^2}\frac{\left(1+\sigma^4\left(\varphi^{(2)}\right)^2\right)}{\left(1+\sigma^4\left(\varphi^{(2)}\right)^2/9\right)}\right]}{\sqrt{\left(1+\sigma^4\left(\varphi^{(2)}\right)^2\right)\left(9+\sigma^4\left(\varphi^{(2)}\right)^2\right)}}. \tag{3.30}$$

This analytical result shows that for Fourier-transform limited input pulse ($\varphi^{(2)} = 0$) the XPW spectrum is $\sqrt{3}$ times broader than that of input pulse. For chirped pulses however ($\varphi^{(2)} \neq 0$), the XPW spectral width narrows with increasing $\varphi^{(2)}$ and is $1/\sqrt{3}$ smaller than the input spectrum for a high spectral chirp. Integrating (3.30) over the frequency domain, one can also obtain the dependence of the XPW pulse energy on the input second order spectral phase coefficient $\varphi^{(2)}$:

$$E_{\mathrm{XPW}}(L,\varphi^{(2)}) = \frac{E_{\mathrm{XPW},0}}{\left(1+\sigma^4\left(\varphi^{(2)}\right)^2\right)} \tag{3.31}$$

where $E_{\mathrm{XPW},0}$ is the XPW energy of the pure Fourier transform limited pulse. As can be seen, this dependence is Lorentzian. From Eq. (3.30) the spectral center of mass is calculated. Applying Eq. (3.22), leads to $<\omega>_{\mathrm{XPW}} = \omega_0$, demonstrating that there is no spectral shift.

From the previous results, two critical second order coefficient values can be defined corresponding respectively to the following conditions: the XPW efficiency is equal to half of the maximum conversion efficiency, the XPW spectrum is equal to the input spectrum. For a Gaussian input pulse, these critical coefficients are given by:

$$\varphi^{(2)}_{\mathrm{cr,Energy}} = \sqrt{3}/\sigma^2 \tag{3.32}$$

$$\varphi^{(2)}_{\mathrm{cr,Width}} = 1/\sigma^2 \tag{3.33}$$

For a Gaussian pulse of minimal pulse duration $\tau_0 = 30\,\mathrm{fs}$ the spectral width at $1/e$ is $\sigma = 55.5\,\mathrm{THz}$ and the corresponding critical second order phase coefficients are $325\,\mathrm{fs}^2$ and $562\,\mathrm{fs}^2$ respectively.

For the more general case of an input polynomial phase, the integration in Eq. (3.27) needs to be solved numerically. This is presented in section 3.4.5. Before doing this a simplified analytical model is derived to understand more easily some aspects of the solutions.

3.4.4 Asymptotic shapes and expressions for the XPW spectrum

Assuming a sufficiently regular and smooth input spectrum (i.e. not necessarily a Gaussian pulse), some features of the XPW spectrum can be described by applying the stationary phase

theorem to expression (3.28). This theorem leads, as I will discuss later, to two different results with two different and complementary ranges of validity. The goal of this model is to understand in a simple way the influence of the residual phase on the XPW spectrum and so to extract information about this phase from the shape of the spectrum. The results of the asymptotic model are confirmed more quantitatively by the numerical calculation. Before entering the heart of the matter, I recall the stationary phase theorem applied to a bidirectional complex function of modulus $a(x, y)$ and phase $\phi(x, y)$. According to the stationary phase theorem, the main contribution terms of the integral

$$\int_{\mathbb{R}^2} a(x,y)e^{i\phi(x,y)}dxdy \tag{3.34}$$

come from the angular frequencies x_0 and y_0 for which the phase of the integrand is locally stationary. If such stationary point exists in the $[x_0, y_0]$ ensemble for a particular value of ω_c, then the XPW spectrum will exhibit a local maximum at angular frequency ω_c. What is more, the theorem also gives the following asymptotic formula when the phase is locally stationary ($\phi'(x_0, y_0) = 0$) but not critical ($\phi''(x_0, y_0) \neq 0$):

$$\int_{\mathbb{R}^2} a(x,y)e^{i\phi(x,y)}dxdy = 2\pi\frac{a(x_0,y_0)e^{i\phi(x_0,y_0)}}{\sqrt{|\phi_{x,x}\phi_{y,y} - \phi_{x,y}\phi_{y,x}|}}e^{i\frac{\pi}{4}\,\mathrm{sign}\,\phi''(x_0,y_0)} + O\left(h^2\right) \tag{3.35}$$

with $\phi_{i,j}$ i,j=x,y are partial derivative evaluated at $(x_0, y_0) = 0$. Moreover, in this and in the following sections, the central angular frequency and spectral width of the cube of the input spectral intensity will be noted $< \omega >_{I_A^3}$ and $\sigma_{I_A^3}$ respectively.

Spectral phase with critical points

Mathematically, the stationary phase condition applied to the integrand of the right hand side of equation (3.28) is:

$$\exists\,(\omega_1, \omega_2) \;\mid\; \frac{d}{d\omega_{1,2}}\left[\varphi(\omega_1) + \varphi(\omega_2) - \varphi(\omega_1 + \omega_2 - \omega)\right] = f_{1,2}(\omega) \tag{3.36}$$

where $f_{1,2}(\omega)$ are two real functions. This condition of local maximum has a more natural expression using the group delays:

$$\begin{cases} \tau(\omega_1) - \tau(\omega_1 + \omega_2 - \omega) = f_1(\omega) \\ \tau(\omega_2) - \tau(\omega_1 + \omega_2 - \omega) = f_2(\omega) \end{cases} \tag{3.37}$$

Although the exact set of solutions of this equation system is unknown in the general case, there is one obvious solution: $\omega_1 = \omega_2 = \omega$. If this solution is the only solution, then, an asymptotic expression of the XPW spectrum is:

$$I_B(\omega) \simeq \frac{I_A(\omega)^3}{|\varphi"(\omega)|^2} \tag{3.38}$$

From a mathematical point of view, the range of validity of the stationary phase is limited to high phase values, that is to say for input pulses which are far from the Fourier-transform limit.

Nevertheless, this approximation proves to be useful. If the fundamental spectral phase exhibits a critical point ($\varphi"(\omega_c) = 0$), then the phase function of equation (3.28) is also critical at ω_c and formula (3.38) cannot be applied around ω_c, which is obvious since the formula diverges at ω_c. However, in such a case, the XPW spectrum can still be described by the sum of two contributions: a "local" contribution given by expression (3.38) (away from ω_c) and a "critical" contribution corresponding to a peak distribution located at ω_c.

An example of this is a spectral phase well described by a third order Taylor expansion around ω_0, then the XPW spectrum is expected to exhibit a maximum at the angular frequency which is solution of:

$$\varphi''(\omega) = \varphi^{(2)} + \varphi^{(3)}(\omega - \omega_0) = 0 \tag{3.39}$$

This analytical approach enables us to predict the following spectral behavior of the XPW spectrum: when there are strong residual second and third order phases on the fundamental pulse, the XPW spectrum is no longer symmetric even for a symmetric input. What is more, the XPW spectrum is the sum of the cube of the input spectrum and a peak at the position:

$$\omega = \omega_0 - \frac{\varphi^{(2)}}{\varphi^{(3)}} \tag{3.40}$$

Since the peak distribution is weighted by the amplitude factor I_A^3, the spectral center of mass is therefore expected to behave as follows:

$$< \omega >_{\mathrm{XPW}} = \omega_0 - \frac{\varphi^{(2)}}{\varphi^{(3)}} I_A^3(\omega_0 - \varphi^{(2)}/\varphi^{(3)})/I_A^3(\omega_0) \tag{3.41}$$

In this particular case, the range of validity of this approximation can be defined as $\sigma_{I_A}^3|\varphi^{(3)}| >> 1$ and $|\varphi^{(2)}| < |\varphi^{(3)}\sigma|$.

Spectral phase without critical points

The stationary phase theorem gives also some asymptotic expressions for the XPW spectrum when there are no critical points for the fundamental pulse. More precisely, if the group delay of the input pulse is monotonic (this is the case if the spectral phase is predominantly quadratic or quartic for example) and if the duration of the fundamental pulse is much longer than its transform-limit, then the XPW modulus of the spectral amplitude is approximately given by the solution in (3.38), over the whole spectral range.

From this result, one can compute, to the first order, the spectral center of mass and spectral width of the XPW spectrum for a chirped input pulse to which a perturbative third order phase has been added:

$$< \omega >_{\mathrm{XPW}} = \omega_0 - 2\frac{\varphi^{(3)}}{\varphi^{(2)}}\sigma_{I_A^3}^2 \tag{3.42}$$

$$\sigma_{\mathrm{XPW}}^2 = \sigma_{I_A^3}^2 - 2\frac{\varphi^{(3)}}{\varphi^{(2)}} < (\omega - \omega_0)^3 >_{I_A^3} \tag{3.43}$$

Applying this result to a linearly chirped pulse ($\varphi^{(3)} = 0$), leads to the same results found in section 3.4.3 for large chirps: the spectrum is narrowed by a factor $\sqrt{3}$, the conversion efficiency

decreases with $1/\left(\varphi^{(2)}\right)^2$. With a perturbative third order phase, the spectral center of mass is shifted proportionally to the $\varphi^{(3)}$ value. As far as the spectral width is concerned, it remains unchanged to the first order if the spectrum is symmetric with respect to the spectral center of mass. If the spectrum is not symmetric, then the spectrum may be broadened or narrowed depending on the relative signs of the phase coefficients.

Again, the range of validity of these approximations needs to be specified. The above results only apply for strongly chirped pulses. For a general cubic phase function, this means $\sigma_{I_A}^2|\varphi^{(2)}| >> 1$ and $|\varphi^{(2)}| >> |\varphi^{(3)}\sigma_{I_A}|$.

Synthesis

This simplified model predicts that, for a sufficiently regular spectrum with a large general cubic phase, the spectral center of mass varies linearly with $\varphi^{(3)}$ for large and constant values of $\varphi^{(2)}$ and linearly with $\varphi^{(2)}$ for large and constant values of $\varphi^{(3)}$. Such features are characteristic of a hyperbolic parabola surface, more widely known as a horse saddle surface and will be obtained experimentally in section 4.6. The saddle point is centered on $\varphi^{(2)} = \varphi^{(3)} = 0$ and can be implicitly defined by the equation $\varphi^{(2)}\varphi^{(3)} = const.$

The spectral width of the XPW spectrum is expected to be almost constant whenever the effects of $\varphi^{(2)}$ or $\varphi^{(3)}$ are dominant. In the first case, the spectral width is equal to that of the cube of the input spectrum. In the second case, it is related to the spectral width of the "critical" contribution. Last, this model confirms a general Lorentzian dependance of the XPW intensity as a function of $\varphi^{(2)}$.

3.4.5 Numerical calculation

In this paragraph I directly solve Eq. (3.28) and compute the XPW spectral intensity without any other assumptions than those stated in section 3.4.2. In order to verify the previous theoretical work, the effect of combined second and third order spectral phases are simulated. The input spectrum is Gaussian with a spectral width corresponding to a Fourier transform limited pulse of 30 fs. The energy, center of mass and spectral width of the XPW spectrum are shown in Fig. 3.15 and Fig. 3.16. For all these scans we choose approximatively $\triangle\varphi^{(2)} = \sigma_{I_A}^2 \triangle\varphi^{(3)}$ to have the same temporal effect for both phase terms.

The main conclusion from Fig. 3.15 is that the plots are symmetric with respect to the point where $\varphi^{(2)} = \varphi^{(3)} = 0$. At this point the XPW generation process exhibits maximum efficiency and the broadest spectrum without spectral shift. Efficiency and broadening decrease with residual spectral phase and one obtains numerically the same values for $\varphi^{(2)}_{\text{cr,Energy}}$ and $\varphi^{(2)}_{\text{cr,Width}}$ been derived analytically previously. As expected, the spectral center of mass of the XPW spectrum (Fig. 3.16 (a)) shifts when the contributions of second and third order phase coefficients are of the same order of magnitude. The numerical calculation provides realistic spectral shifts that can be used to compare with experimental data. For comparison,

Fig. 3.16 (b) presents the spectral shift behavior extracted from the analytical model for the same spectral phase range as Fig. 3.16 (a). They both behave the same, but the numerical calculation provides realistic spectral shifts for Gaussian laser spectra compared to the analytical model. Furthermore the analytical model is not valid at the saddle point in the center of the graph.

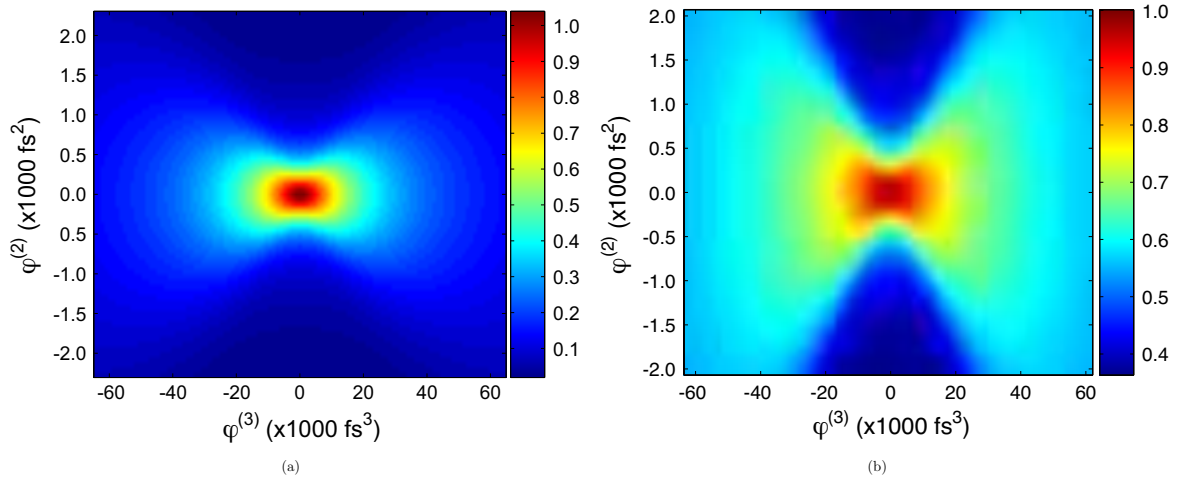

Figure 3.15: (a) normalized theoretical XPW efficiency function of the second and third order spectral phase for a 30 fs input pulse. The value 1 corresponds to a XPW efficiency of 5%. (b) theoretical prediction of XPW spectral width as a function of the second and third order spectral phases for a 30 fs pulse. The spectral width values are normalized to the XPW width value for the case of transform limited input pulse.

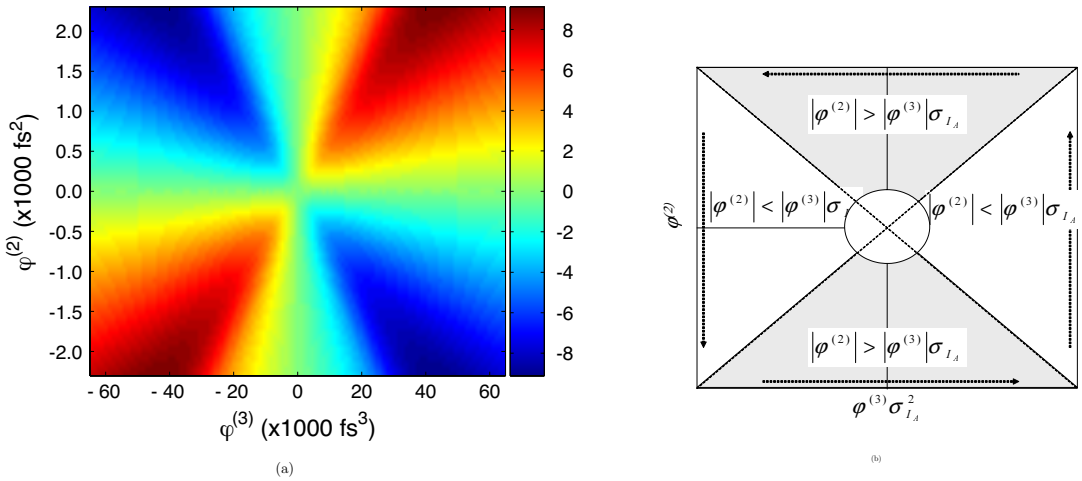

Figure 3.16: (a) theoretical prediction of the XPW spectral center of mass shift (in nm) as a function of the second and third order spectral phases for a 30 fs input pulse. (b) validity range of the two approximations in the $\left(\varphi^{(2)}(\omega_0), \varphi^{(3)}(\omega_0)\right)$ plane for the analytical model. The arrows show the direction of the spectral center of mass shift for a cubic spectral phase.

These theoretical predictions are verified experimentally in section 4.6.

3.4.6 XPW generation for sub-10 fs pulses

In the previous derivation the pulse dispersion during the propagation in the nonlinear medium has been neglected. For pulses shorter than 10 fs this is not valid anymore because dispersion and nonlinearity act together during propagation. This implies solving a nonlinear partial differential system of equations instead of a system of ordinary differential equations. The split-step Fourier method provides an approximate solution of this system by assuming that in propagating the optical field over a small distance h, the dispersive and nonlinear effects can be considered to act independently of each other. More specifically, propagation from z to z+h is carried out in two steps. In the first step the nonlinearity acts alone and the coupled nonlinear equations (3.9) are solved in time domain. In the second step dispersion acts alone and the spectral phase from material dispersion is applied in the frequency domain. Fig. 3.17 illustrates the dynamics of the XPW conversion process for three selected values for the residual chirp at the entrance of the crystal (1 mm) : 0 (a,b,c), -25 fs^2 (d,e,f), -60 fs^2 (g,h,i). Fig. 3.17 (a,d,g) shows the evolution of the temporal shape of the fundamental as it propagates through the crystal. For a short input pulse (8 fs in the simulation), the extremely wide bandwidth (we used a spectrum typical for spectral broadening in a hollow fiber) of the pulse results in a rapid broadening, even though the crystal is quite thin (Fig. 3.17a). For a slight negative input chirp ($-25f^2$), the pulse is temporally focused near the center of the crystal(Fig. 3.17d). If the input chirp is further decreased, the pulses compresses in the last 200 μm of the crystal(Fig. 3.17g). As the pulse compresses, the central wavelength of the shortest part of the pulse varies, resulting in a shift in the pulse peak, since the temporal window of the calculation moves at the group velocity of the 800 nm pulse. The moderate input intensity and rapid pulse broadening gives little self-phase modulation on the input spectrum. The remaining panels in Fig. 3.17 show the evolution of the XPW signal in the temporal (Fig. 3.17(b,e,h)) and spectral domains (Fig. 3.17(c,f,i)). The corresponding beam-integrated output spectra are shown in Fig. 3.18. Since the XPW pulse is initially quite short, it broadens over a very short distance (Fig. 3.17(b,e)). For the short pulse input, the conversion starts early in the crystal, and by the middle of the crystal the spectrum is very broad and smooth (Fig. 3.17(c)). Subsequent conversion takes place with a positively chirped pulse, leading to the evolution of the double humped output spectrum (Fig. 3.18). For a negatively-chirped input pulse, the pulse is temporally focused in the center of the crystal, there is some initial conversion on the initially chirped pulse, allowing a greater portion of the output energy to result from conversion of the short pulse. This results in a smoother output spectrum and better energy conversion (Fig. 3.17(f)). With the greater value of negative chirp ($-60fs^2$) (Fig. 3.17(i)) such that the temporal focus is near the exit face of the crystal, the output spectrum is somewhat narrower and the conversion efficiency is greatly reduced (Fig. 3.18). In this case, most of the conversion occurs with a negatively chirped pulse. Fig. 3.18 also shows the ideal output spectrum for dispersion free conversion calculated with a flat input spectral phase. Clearly the output spectra are limited by the crystal dispersion. Such very broad spectrum could be produced by using very thin crystals (< 100 μm), at the expense of the conversion efficiency.

The calculations suggest that a crystal thickness of 300-500 μm would give a good compromise between output spectrum and conversion efficiency.

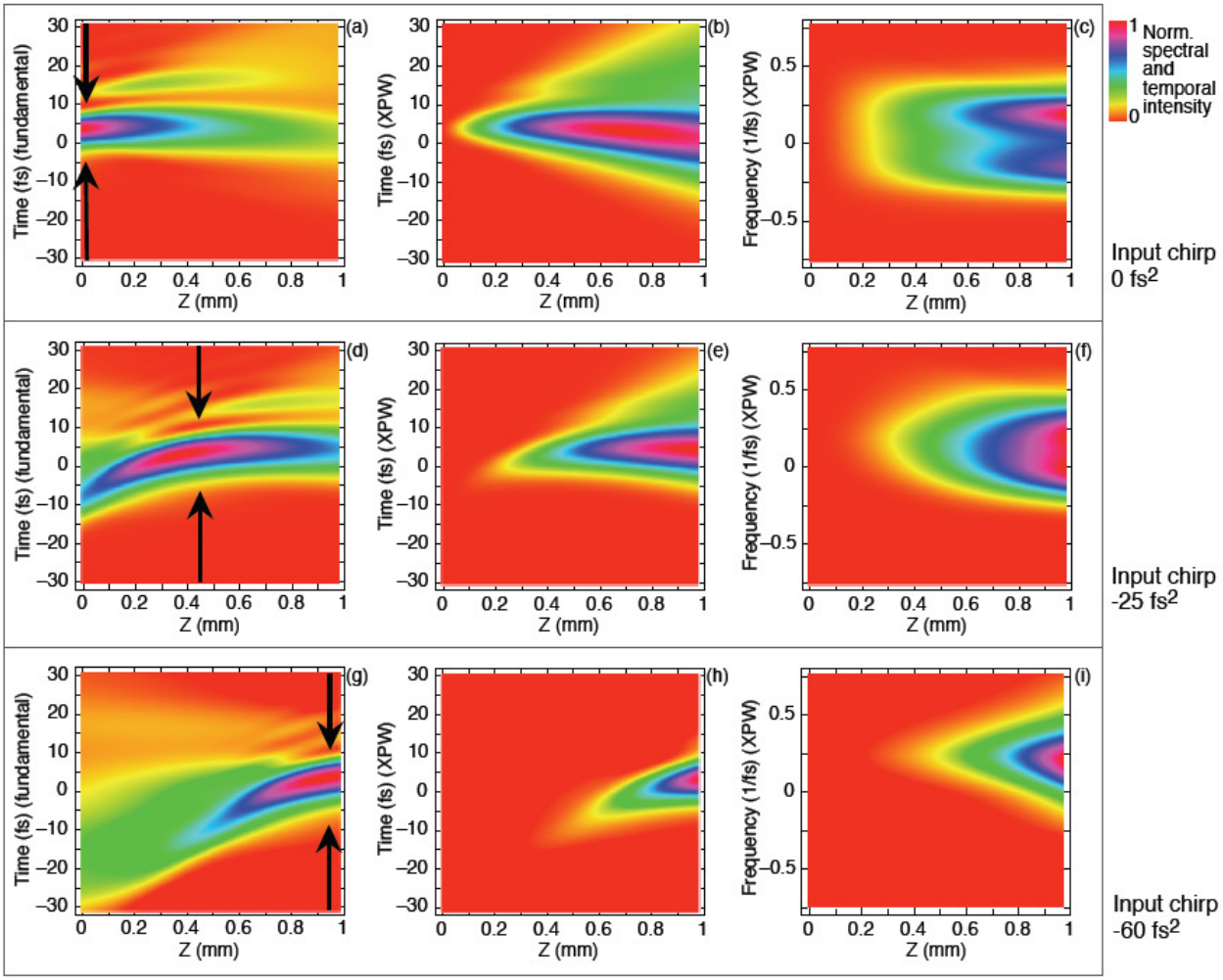

Figure 3.17: Calculated dynamics of XPW generation process. The temporal evolution of the fundamental (resp.XPW) pulse when propagating through the crystal is represented in Figs (a,d,g)(resp.(b,e,h). Figures (c,f,i) display the spectral evolution of the XPW signal within the crystal. Temporal and spectral intensities are normalized. The black arrows localize the area in the crystal where the fundamental beam is temporally the shortest. Panels (a,b,c) are calculated for no residual chirp (0 fs^2) at the entrance of the crystal. -25 fs^2 input chirp is taken into account for figures (d,e,f), and -60 fs^2 input chirp for figures (g,h,i). This values of the residual chirp are typical after hollow fiber spectral broadening and compression and comparison with experiments can thus be done.

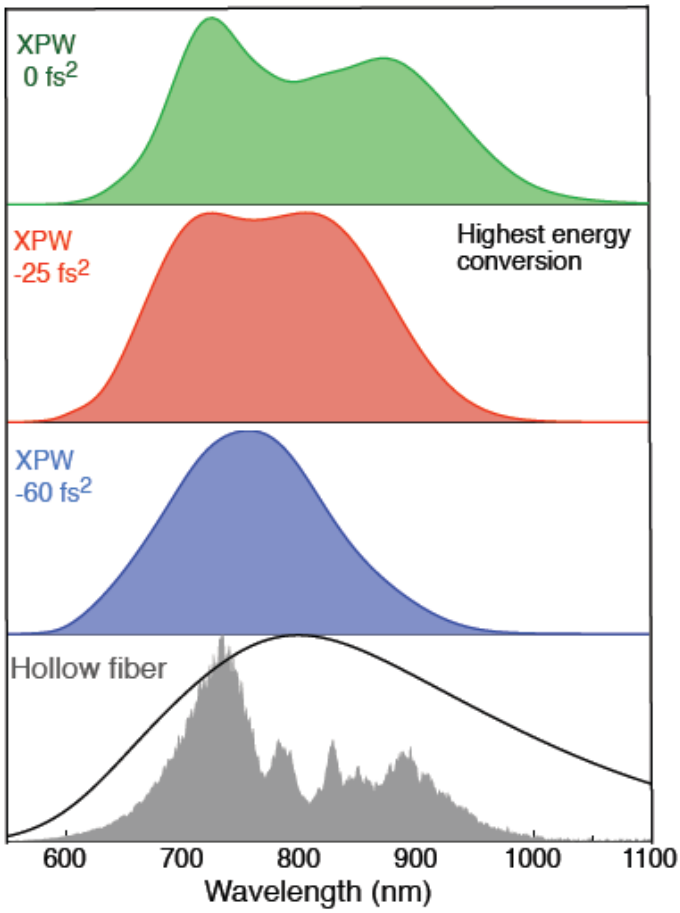

Figure 3.18: Calculated XPW spectra (extracted from Fig. 3.17(a,f,i)) for selected values of the input chirp. The experimental hollow fiber spectrum used for calculations is also shown (grey area, lower panel). The calculated XPW spectrum for a dispersion free conversion and flat input spectral phase is plotted in the lower panel (black line)

Up to now, all the theoretical equations discussed in this chapter have the SVEA approximation as a starting point. For short pulses this approximation implies that the envelope varies slowly over an optical cycle and this is certainly not verified for few-cycle pulses. For such short pulses it is not even evident that the separation of the electric field in a carrier and an envelope is acceptable. The validity of this assumption together with the slowly evolving wave approximation (SEWA) was discussed by Brabec and Krausz in [23]. In this approximation there are no conditions specifying the slowness of the temporal change of the envelope compared with the optical cycle time but it is required that the wave packet has small changing along a propagation distance equal to the wavelength. This can be extended to nonlinear frequency mixing as long as the difference between phase and group velocities of the waves involved in the interaction is small compared to the phase (or group) velocity of the fundamental. This is verified in the case of XPW generation. Within this approximation, a first-order propagation equation for the wave envelope, valid to the single cycle regime, is given by the expression:

$$\left[\partial_z - ik(\omega)\right]\tilde{E}(r,\omega) = \frac{i}{2k(\omega)}\nabla_\perp^2\tilde{E}(r,\omega) - \frac{i\omega}{2\epsilon_0 n(\omega)c}\hat{F}\left[\tilde{P}_{nl}(r,t)\right] \tag{3.44}$$

Compared with the equation derived with SVEA it contains new terms which are responsible for effects like self-steepening and space-time focusing. This equation with the nonlinear contribution from XPW generation can be solved using the Fourier split step method presented previously. This falls within the frame of further investigations.

Bibliography

[1] N. Minkovski, G. I. Petrov, S. M. Saltiel, O. Albert, and J. Etchepare. Nonlinear polarization rotation and orthogonal polarization generation experienced in a single-beam configuration. *J. Opt. Soc. Am. B* **21**, 1659 (2004)

[2] A. Jullien, O. Albert, F. Burgy, G. Hamoniaux, J.-P. Rousseau, J.-P. Chambaret, F. Augé-Rochereau, G. Chériaux, J. Etchepare, N. Minkovski, and S. M. Saltiel. 10^{-10} temporal contrast for femtosecond ultraintense lasers by cross-polarized wave generation. *Opt. Lett.* **30**, 920 (2005)

[3] V. Chvykov, P. Rousseau, S. Reed, G. Kalinchenko, and V. Yanovsky. Generation of 10^{11} contrast 50 TW laser pulses. *Opt. Lett.* **31**, 1456 (2006)

[4] L. Canova, M. Merano, A. Jullien, G. Chériaux, R. Lopez-Martens, O. Albert, N. Forget, S. Kourtev, N. Minkovsky, and S. M. Saltiel. Coherent contrast improvement by cross-polarized wave generation. In Conference on Lasers and Electro-Optics/Quantum Electronics and Laser Science Conference and Photonic Applications Systems Technologies **JThD131** (2007)

[5] M. Kalashnikov, K. Osvay, and W. Sandner. High-power Ti:Sapphire lasers: Temporal contrast and spectral narrowing. *Laser and Particle Beams* **25**, 219 (2007)

[6] M. P. Kalashnikov, K. Osvay, I. M. Lachko, H. Schönnagel, and W. Sandner. Suppression of gain narrowing in multi-tw lasers with negatively and positively chirped pulse amplification. *Appl. Phys. B*, **81**, 1059 (2005)

[7] T. Oksenhendler, D. Kaplan, P. Tournois, G. M. Greetham, and F. Estable. Intracavity acousto-optic programmable gain control for ultra-wide-band regenerative amplifiers. *Appl. Phys. B*, **83**, 491 (2006)

[8] H. Takada and K. Torizuka. Design and construction of a tw-class 12-fs ti:sapphire chirped-pulse amplification system. *Selected Topics in Quantum Electronics, IEEE Journal of*, **12**, 201 (2006)

[9] I. Pastirk, B. Resan, A. Fry, J. MacKay, and M. Dantus. No loss spectral phase correction and arbitrary phase shaping of regeneratively amplified femtosecond pulses using miips. *Optics Express*, **14**, 9537 (2006)

[10] A. Jullien, L. Canova, O. Albert, D. Boschetto, L. Antonucci, Y.-H. Cha, J. P. Rousseau, P. Chaudet, G. Chériaux, J. Etchepare, S. Kourtev, N. Minkovski, and S. M. Saltiel. Spectral broadening and pulse duration reduction during cross-polarized wave generation: influence of the quadratic spectral phase. *Appl. Phys. B* **87**, 595 (2007)

[11] M. P. Kalashnikov, E. Risse, H. Schönnagel, and W. Sandner. Double chirped-pulse-amplification laser: a way to clean pulses temporally. *Opt. Lett.* **30**, 923 (2005)

[12] M. E. Anderson, L. E. E. de Araujo, E. M. Kosik, and I. A. Walmsley. The effects of noise on ultrashort-optical-pulse measurement using spider. *Appl. Phys. B* **70**, S85 (2000)

[13] D. N. Fittinghoff, K. W. DeLong, R. Trebino, and C. L. Ladera. Noise sensitivity in frequency-resolved optical-gating measurements of ultrashort pulses. *J. Opt. Soc. Am. B* **12**, 1955 (1995)

[14] G. Stibenz, C. Ropers, C. Lienau, C. Warmuth, A. S. Wyatt, I. A. Walmsley, and G. Steinmeyer. Advanced methods for the characterization of few-cycle light pulses: a comparison. *Appl. Phys. B*, **83**, 511 (2006)

[15] E. Sidick, A. Dienes, and A. Knoesen. Ultrashort-pulse second-harmonic generation. non-transform-limited fundamental pulses. *J. Opt. Soc. Am. B* **12**, 1713 (1995)

[16] A. C. L. Boscheron, C. J. Sauteret, and A. Migus. Efficient broadband sum frequency based on controlled phase-modulated input fields: theory for 351-nm ultrabroadband or ultrashort-pulse generation *J. Opt. Soc. Am. B*, **13**, 818 (1996)

[17] K. Osvay and I. N. Ross. Broadband sum-frequency generation by chirp-assisted group-velocity matching. *J. Opt. Soc. Am. B*, **13**, 1431 (1996)

[18] G. Veitas and R. Danielius. Generation of narrow-bandwidth tunable picosecond pulses by difference-frequency mixing of stretched pulses. *J. Opt. Soc. Am. B*, **16**, 1561 (1999)

[19] P. Baum, S. Lochbrunner, and E. Riedle. Generation of tunable 7-fs ultraviolet pulses: achromatic phase matching and chirp management. *Appl. Phys. B* **79**, 1027 (2004)

[20] C. Iaconis and I. A. Walmsley. Spectral phase interferometry for direct electric-field reconstruction of ultrashort optical pulses. *Opt. Lett.* **23**, 792 (1998)

[21] F. Verluise, V. Laude, Z. Cheng, Ch. Spielmann, and P. Tournois. Amplitude and phase control of ultrashort pulses by use of an acousto-optic programmable dispersive filter: pulse compression and shaping. *Opt. Lett.* **25**, 575 (2000)

[22] A. Baltuška, T. Fuji, and T Kobayashi. Controlling the carrier-envelope phase of ultrashort light pulses with optical parametric amplifiers. Phys. Rev. Lett., 88(13):133901

[23] T. Brabec and F Krausz. Intense few-cycle laser fields: Frontiers of nonlinear optics. *Rev. Mod. Phys.*, 72(2):545–591, Apr 2000.